NeuroImage 120 (2015) 75–87

Contents lists available at ScienceDirect

NeuroImage

journal homepage: www.elsevier.com/locate/ynimg

Task- and stimulus-related cortical networks in language production: Exploring similarity of MEG- and fMRI-derived functional connectivity

Mia Liljeström [a,b,c,d,*,1], Claire Stevenson [a,b,1], Jan Kujala [a,b], Riitta Salmelin [a,b]

[a] Department of Neuroscience and Biomedical Engineering, Aalto University, Espoo, Finland
[b] Aalto NeuroImaging, Aalto University, Espoo, Finland
[c] Department of Neurological Sciences, Helsinki University, Helsinki, Finland
[d] Department of Neurology, Helsinki University Central Hospital, Helsinki, Finland

ARTICLE INFO

Article history:
Received 29 October 2014
Accepted 7 July 2015
Available online 11 July 2015

Keywords:
MEG
fMRI
Functional connectivity
Connectome
Task networks
Picture naming

ABSTRACT

Large-scale networks support the dynamic integration of information across multiple functionally specialized brain regions. Network analyses of haemodynamic modulations have revealed such functional brain networks that show high consistency across subjects and different cognitive states. However, the relationship between the slowly fluctuating haemodynamic responses and the underlying neural mechanisms is not well understood. Resting state studies have revealed spatial similarities in the estimated network hub locations derived using haemodynamic and electrophysiological recordings, suggesting a direct neural basis for the widely described functional magnetic resonance imaging (fMRI) resting state networks. To truly understand the nature of the relationship between electrophysiology and haemodynamics it is important to move away from a task absent state and to establish if such networks are differentially modulated by cognitive processing. The present parallel fMRI and magnetoencephalography (MEG) experiment investigated the structural similarities between haemodynamic networks and their electrophysiological counterparts when either the stimulus or the task was varied. Connectivity patterns underlying action vs. object naming (task-driven modulations), and action vs. object images (stimulus-driven modulations) were identified in a data driven all-to-all connectivity analysis, with cross spectral coherence adopted as a metric of functional connectivity in both MEG and fMRI. We observed a striking difference in functional connectivity between conditions. The spectral profiles of the frequency-specific network similarity differed significantly for the task-driven vs. stimulus-driven connectivity modulations. While the greatest similarity between MEG and fMRI derived networks was observed at neural frequencies below 30 Hz, haemodynamic network interactions could not be attributed to a single frequency band. Instead, the entire spectral profile should be taken into account when assessing the correspondence between MEG and fMRI networks. Task-driven network hubs, evident in both MEG and fMRI, were found in cortical regions previously associated with language processing, including the posterior temporal cortex and the inferior frontal cortex. Network hubs related to stimulus-driven modulations, however, were found in regions related to object recognition and visual processing, including the lateral occipital cortex. Overall, the results depict a shift in network structure when moving from a task dependent modulation to a stimulus dependent modulation, revealing a reorganization of large-scale functional connectivity during task performance.

Introduction

It is generally thought that human cognition is mediated by a set of interconnected distributed neural networks rather than spatially focal brain responses (Mesulam, 1990; Varela et al., 2001). Consequently, with the advance of signal processing techniques, the field of functional neuroimaging is moving towards a network based approach to data analysis (e.g. Achard et al., 2006; Hutchison et al., 2013; Salvador et al., 2005; Stam, 2004). One of the most widely used techniques for functional mapping of human brain activity is blood oxygenation level dependent (BOLD) functional magnetic resonance imaging (fMRI) (Ogawa et al., 1990), which allows for mapping of brain-wide haemodynamic modulations with high spatial resolution (typically millimetres). Network analyses of these haemodynamic modulations at rest have revealed functional networks in the brain (Biswal et al., 1995; Fox and Raichle, 2007; van den Heuvel and Hulshoff Pol, 2010) that show high

* Corresponding author at: Department of Neuroscience and Biomedical Engineering, Aalto University, Espoo, Finland PO BOX 15100, 00076 Aalto, Finland. Fax: +358 9 470 22969.
E-mail address: mia.liljestrom@aalto.fi (M. Liljeström).
[1] Authors contributed equally to this work.

http://dx.doi.org/10.1016/j.neuroimage.2015.07.017

consistency across subjects, studies and cognitive states (Fox and Raichle, 2007; Smith et al., 2009). Recent studies have further indicated that functional networks undergo modulation during task performance (Arbabshirani et al., 2013; Betti et al., 2013; Liljeström et al., 2015; Saarinen et al., 2015; Xu et al., 2014).

Since BOLD fMRI is an indirect measure of neural activity, much work has been undertaken in understanding the coupling mechanisms which relate the underlying electrophysiology to the haemodynamic response (Logothetis et al., 2001; Rosa et al., 2011). Such an understanding is crucial to a full and correct interpretation of neuroimaging data and a true appreciation of the way in which the brain processes information. Non-invasive measures of electrophysiological activity can be obtained with magnetoencephalography (MEG; Cohen, 1968; Hämäläinen et al., 1993) and electroencephalography (EEG; Pfurtscheller and Lopes da Silva, 1999), which provide millisecond temporal resolution of brain activity but at a lower spatial resolution than fMRI BOLD. Several studies have investigated the association between task-related changes in electrophysiological activity (measured using MEG or EEG) and the haemodynamic response (measured with fMRI), providing somewhat conflicting results. For low-level sensory stimuli, activation peaks in BOLD fMRI data show a good spatial correspondence with task-related changes in electrophysiological power (Brookes et al., 2005; Stevenson et al., 2012). However, the results for task-related amplitude correlation between electrophysiological and haemodynamic effects are somewhat inconsistent (Muthukumaraswamy and Singh, 2009; Winterer et al., 2007). In more cognitively demanding tasks, studied across multiple brain regions, a large degree of variability in the correspondence between haemodynamics and electrophysiology is found (Kujala et al., 2014; Liljeström et al., 2009; Vartiainen et al., 2011), with both spatial and functional discrepancies between MEG and fMRI becoming more apparent. Such findings are evident also with invasive electrophysiological recordings (Conner et al., 2011).

If large-scale distributed networks do indeed mediate human cognition, comparison of the entire haemodynamic and electrophysiological task network, rather than confining evaluations to areas of maximal activity, is needed for a full description of the relationship between haemodynamic and electrophysiological effects. Recent work has shown spatial similarities between resting state network hubs obtained from M/EEG and fMRI data (Brookes et al., 2011b; de Pasquale et al., 2010, 2012; Mantini et al., 2007; Tal et al., 2013; Tewarie et al., 2014). However, if we aim for a comprehensive account of the mechanism by which distributed neural assemblies interact to perform specific functions, investigations into how measures of functional connectivity are affected by task execution are required.

In the current work, we examined task-related modulations in global connectivity patterns in a parallel MEG/fMRI cognitive experiment, where the same subjects participated in both recordings. As a metric of functional connectivity we adopt spectral coherence in both MEG and fMRI. Coherence of cortical oscillatory neural activity, here measured with MEG, has long been proposed as a mechanism for information transfer within the human brain (Engel et al., 1999; Fries, 2005). Previous studies have suggested that individual spectral components of the broadband MEG signal may have functionally specific roles with respect to both long-range and short-range binding and in terms of the relationship with the haemodynamic response (Buffalo et al., 2011; Donner and Siegel, 2011; Hipp et al., 2012). To match the MEG analysis as closely as possible we chose coherence as a measure for connectivity also in fMRI. Furthermore, it has been shown that interregional dependencies in fMRI data are more readily observed in the frequency than time domain, and recent work (Lohmann et al., 2010; Wu et al., 2008) suggests that functionally relevant information may be contained in individual frequency components of the low-frequency BOLD response. If so, we may expect to find frequency-specific fMRI networks that correlate differentially with their electrophysiological counterparts. We thus examined the network modulations on the cortical surface for both MEG and fMRI data across a range of frequencies.

To study cognitively relevant large-scale functional connectivity we used picture naming as a task, probing the cortical representations of action and object naming (Liljeström et al., 2008, 2009). Picture naming recruits multiple brain areas within the occipital, temporal, parietal and frontal cortices bilaterally (Indefrey and Levelt, 2004; Salmelin et al., 1994), thus providing a unique viewpoint from which to study the assembly of long-range neural networks necessary for task execution. The nature of the stimuli used here (action images, object only images) allowed for subtle modulations of both stimuli and task to manipulate the formation of the cognitive networks. The experiment was split into two broad categories, (i) presentation of identical visual stimuli with participants required to undertake subtly different tasks, i.e. silent naming of words from different grammatical categories (verbs/nouns) in response to pictures depicting an action, and (ii) presentation of differing visual stimuli with participants required to execute identical tasks, i.e. consistently naming words from the same grammatical category (nouns) in response to pictures depicting either an action or an object only. This setup facilitated comparisons of MEG and fMRI task-related network hubs, as well as evaluation of possible distinctions in MEG–fMRI correspondence between stimulus and task dependent connectivity modulations.

We hypothesized that if there is a correspondence between the haemodynamic and electrophysiological networks then the spatial locations of cortical hubs should be shared between modalities and the manner in which the connections are modulated by stimuli or task should be comparable. We also aimed to establish whether a dominant frequency band of MEG connectivity data exists which most closely corresponds to the haemodynamic networks.

Materials and methods

Subjects and data acquisition

15 healthy subjects (8 males and 7 females, mean age 25 years, range 19–32 years; 14 right-handed, one ambidextrous) gave their informed consent to participate in the study in agreement with a prior approval of the local Ethics Committee (Hospital district of Helsinki and Uusimaa). The participants all had normal or corrected-to-normal vision, had no history of psychiatric or neurological disorders, and were native Finnish speakers. Both functional MRI data and MEG data were acquired in 11 subjects. The remaining 4 subjects completed only the fMRI component of the experiment.

MR images were acquired using a Signa VH/i 3.0 T MRI scanner (GE Healthcare, UK). Functional data was acquired using a single-shot gradient-echo planar imaging (GRE-EPI) sequence with the following parameters: TR 3 s, TE = 32 ms, FA = 90, in-plane resolution 3.4 mm × 3.4 mm (7 subjects) or 3 mm × 3 mm (8 subjects), slice thickness 3 mm. Anatomical images were acquired with a T1-weighted 3D spoiled gradient echo (SPGR) sequence.

MEG data were measured using a 306 channel Vectorview MEG device (Elekta, Helsinki, Finland). Eye blinks and saccades were monitored using two electrodes placed diagonally near the lower and upper eye lids (electro-oculograms) and mouth movements were monitored using electrodes placed near the upper and lower lip margins (electromyograms). Head position indicator coils were used to determine the position of the head in relation to anatomical landmarks and to the sensor array. At the beginning of each session the position of the head with respect to the sensors was measured. MEG signals were filtered at 0.03–200 Hz and sampled at 600 Hz.

Experimental paradigm

Subjects silently named actions or objects from simple line drawings. Images were presented with an interstimulus interval of 1.8–4.2 s (stimulus duration 300 ms) in blocks of 10 images (or trials) per block. Each 30-s block was followed by a 21-s rest period. The

experimental setup was identical during the MEG and fMRI recordings (Liljeström et al., 2009). The experiment was divided into 15-min sessions with a short break between sessions. The experiment comprised three different conditions with a total of 100 trials in each condition: (i) action naming from action images (ii) object naming from action images and (iii) object naming from object only images. The stimulus materials are described in detail in (Liljeström et al., 2008). For the purposes of the current study, conditions were split into two contrasts; action and object naming from action pictures, where the visual stimulus was identical for both types of word production, and object naming from action and object images, where the subjects were asked to produce the same type of word each time but the visual stimulus differed. These contrasts will be referred to throughout the manuscript as; 'identical visual stimuli, different naming tasks' and 'identical naming tasks, different visual stimuli', respectively.

Determination of cortical grid space

MEG and fMRI functional connectivity processing streams were matched as closely as possible. To eliminate any confounds due to variations in node number (Zalesky et al., 2010), the same source space grid was used in the fMRI and MEG analyses. To form the grid space, the cortical gray matter in one individual was covered with a regular grid of 7-mm side length, limited to 2 cm from the surface of the brain. All nodes were limited to the cortical grey matter. Grid points located in the anterior frontal and temporal cortex were excluded to avoid any residual effects of eye movements in the MEG data analysis. This grid was then transformed to each individual to create a comparable grid space across subjects. The final grid locations (1826 nodes per individual) were transformed into MNI coordinates for fMRI analysis and data visualization.

MEG data analysis

Preprocessing

Preprocessing of the MEG data included application of the Temporal Signal Space Separation (tSSS) method (Taulu and Simola, 2006) for artifact removal. To compensate for head movements between measurement sessions the measured (noncontinuous) head positioning data was used to transform the MEG data across sessions to the same reference positions (Elekta Maxfilter software package). Epochs containing eye blinks or saccades (rejection limit 150 μV, based on the measured electro-oculograms) were removed. MEG data analysis was performed in 2-Hz frequency bins spanning the frequency range 1–90 Hz, and averaged across predefined frequency bands. Ten different frequency bands were chosen (1–3 Hz, 3–7 Hz, 7–13 Hz, 13–17 Hz, 17–25 Hz, 25–31 Hz, 31–39 Hz, 39–47 Hz, 52–60 Hz, 60–90 Hz; the 50–Hz line noise was excluded), similarly to Liljeström et al. (2015); the frequency bins at both the low and high edge frequency were included in each band. This selection was based on the extensive literature on electrophysiologically measured brain rhythms (for example, Gross et al., 2013b; Jensen et al., 2012; Palva and Palva, 2007; Pfurtscheller and Lopes da Silva, 1999; Salmelin and Hari, 1994; van Wijk et al., 2012). We chose a single frequency band for the delta (1–3 Hz), theta (3–7 Hz), and alpha (7–13 Hz) frequency bands. The beta frequency band (Pfurtscheller and Lopes da Silva, 1999) was divided into a low beta (13–17 Hz; Hipp et al., 2012) and two high-beta (17–25 Hz, 25–31 Hz) frequency bands. We chose a gamma frequency range that was within the range of frequencies often observed for pyramidal–interneuronal network gamma (31–90 Hz; Whittington et al., 2000) and divided it into low gamma (31–39 Hz, 39–47 Hz) and high gamma (52–60 Hz, 60–90 Hz). Data were checked at the sensor level that there was no significant difference in task-related power in the 50–800 ms time-window after stimulus onset between conditions in any frequency band (paired Student's *t*-test, $p < 0.01$) at 99% of the sensors (max 3 sensors with a difference). Importantly, we tested for power differences separately at each sensor to ensure that the spatial power pattern was similar in both conditions.

Connectivity analysis

For reconstruction of coherent sources we used an event-related spatial filter (erDICS, event-related Dynamic Imaging of Coherent Sources; Laaksonen et al., 2008) which can be applied both to localizing source power (Laaksonen et al., 2012) and coherence (Liljeström et al., 2015). One benefit of using this approach is that estimation of regional time-courses is not necessary — the frequency-domain spatial filter (or beamformer) maps the coherence between brain regions directly at the cortical level. Initially, a time–frequency representation for each epoch was calculated using Morlet wavelets of width 7. For each task condition, cross-spectral density matrices (CSDs) across all planar gradiometer channels were computed using the time–frequency representations of the trial time series (50–800 ms after stimulus onset). The sensor-level data, represented by the CSD matrix, was transformed into a cortical representation using the spatial filter. A spherical head conductor model, determined individually for each subject, was used in the source reconstruction.

In an all-to-all connectivity analysis (Liljeström et al., 2015; Saarinen et al., 2015), coherence estimates were computed for each cortical grid point with all other grid points in the frequency bands of interest. For each cortico-cortical connection the source orientation configuration was determined by identifying the orientation combination for the two sources that maximizes their mutual coherence (Liljeström et al., 2015; Saarinen et al., 2015). The orientation pairs were tested for all possible combinations between 50 regularly spaced orientations (spanning 180°, in steps of 3.6°), in the tangential source space with respect to a sphere with origin at the centre of the brain, at both ends of the connection.

Task-related network modulations were determined by contrasting all-to-all connectivity results between conditions (paired Student's *t*-test; $p < 0.0005$) and applying a spatial pairwise clustering algorithm (cluster size 3) that required both ends of a given connection to be within 2 cm of the start and end points of its cluster companions (analogous to Zalesky et al., 2012). As the MEG source space is inherently smooth, special care must be taken to avoid spurious connectivity results due to spatial spread. These effects are highly dependent on the source strength of the underlying sources (Kujala et al., 2008; Schoffelen and Gross, 2009). We therefore used power-matched conditions and assessed changes in connectivity strength between conditions, rather than estimating the connectivity in one condition alone (Kujala et al., 2008; Gross et al., 2013a). We thus make the assumption that the field spread effects are the same in the two experimental conditions, at each location. Although matching the power across conditions is an important step for minimizing effects of spatial spread, it may not completely abolish these effects. We therefore used a minimum distance limit of 4 cm between connection start- and endpoints, which was applied to avoid any remnant spurious connectivity between closely situated regions (similarly to Kujala et al., 2008; Liljeström et al., 2015; de Pasquale et al., 2012).

fMRI data analysis

Preprocessing

FMRI data from all subjects were realigned and tissue segmentation was applied in SPM8 (http://www.fil.ion.ucl.ac.uk/spm/). Constant and linear trends, motion parameters, average white matter and cerebrospinal fluid time courses were regressed out (Behzadi et al., 2007). Data were smoothed (8 mm FWHM Gaussian kernel) and spatially normalized to the SPM8 MNI template. Nodal timecourses were extracted, segmented by task, mean centered, windowed (tapered cosine) and concatenated into blocks of individual task conditions (as in Sun et al., 2004).

Functional connectivity estimates were calculated in 10 subjects, who had all participated also in the MEG part of the experiment. Data from the remaining 5 subjects were used to determine the frequency bands of interest for the functional connectivity analysis. To this end, regional timecourses based on the AAL parcellation scheme were used in the calculations and spectral power estimates were contrasted between task conditions for all anatomical regions. Frequency bands displaying a variance in task-related power change of >10% (see Inline Supplementary Figure S1) were excluded from further analysis to avoid spurious coherence modulations. Frequency bands selected for functional connectivity estimates were; 0.001–0.023 Hz, 0.041–0.061 Hz, 0.07–0.09 Hz and 0.11–0.14 Hz (Inline Supplementary Figure S1).

Inline Supplementary Fig. S1 can be found online at http://dx.doi.org/10.1016/j.neuroimage.2015.07.017.

Connectivity analysis

In an all-to-all connectivity analysis, coherence estimates were computed for each cortical grid point with all other grid points in the frequency bands of interest using Welch's periodogram method. Similarly to the approach adopted for the MEG connectivity analysis, task-related network modulations were determined by contrasting the all-to-all connectivity results between tasks (paired Student's *t*-test; $p < 0.0005$) and applying a spatial pairwise clustering algorithm (cluster size 3) that required both ends of a given connection to be within 2 cm of the start and end points of its cluster companions (analogous to Zalesky et al., 2012). This clustering technique reduces the number of spurious connections. Short-range connections (closer than 4 cm) were excluded to enable comparisons with the MEG-derived networks.

Comparison of MEG and fMRI functional connectivity networks

Topological properties of a network are inherently dependent on the number of edges in the network (or wiring cost) and thresholding is therefore critical when comparing networks from different modalities (Achard and Bullmore, 2007; Ginestet et al., 2011, 2014; van Wijk et al., 2010). The wiring cost *K* of an unweighted network is defined as the number of edges in the network in proportion to all possible connections (N(N − 1) / 2) between N regions. To compare networks across imaging modalities we adapted an approach that matches the MEG and fMRI networks based on cost.

Firstly, we chose a fixed statistical threshold ($p < 0.0005$, with cluster size 3 based on the spatial pairwise clustering algorithm by Zalesky et al., 2012), for the MEG and fMRI connectivity results. Automated Anatomic Labeling (AAL) (Tzourio-Mazoyer et al., 2002) was used to parcellate the cortex into 77 anatomical regions (Fig. 1). MNI (Montreal Neurological Institute) coordinates of the grid locations were used in assigning an anatomical label to each grid point based on the cortical parcellation scheme. Reduced adjacency matrices were then created for both fMRI and MEG data. The data were represented by a weighted adjacency matrix C_{ij}, with each matrix row and column index i, j corresponding to one of the AAL cortical regions covered by the grid. Each matrix element value $C_{ij}(i,j)$ depicts the number of significant connections at the group level between the cortical regions i and j (connection density). The resulting network structures can be visualized using a circular diagram (Fig. 1).

We then performed an overall comparison between MEG and fMRI network structures by averaging the reduced adjacency matrices across frequencies. To match the MEG and fMRI networks we integrated over the cost interval $0.01 < K < 0.1$ (in steps of 0.01), corresponding to 1–10% of a fully connected network. For visualization of the average networks, and their overlap, we chose the cost interval $0.01 < K < 0.05$. At each cost level we created unweighted MEG and fMRI adjacency matrices by taking the top connections in terms of connection density. Any direct overlap of these edges between MEG and fMRI networks was defined as shared connections between the two modalities (similarly to Tewarie et al., 2014). To quantify the overlap between the MEG and fMRI average networks we calculated the Jaccard coefficient of similarity (e.g. Fuxman Bass et al., 2013) at costs ranging from 0.01 to 0.1 (in steps of 0.01). The Jaccard coefficient describes the fraction of overlapping edges (intersection) between the MEG and fMRI networks as compared to the union of edges in the MEG and fMRI networks. To calculate the Jaccard coefficient we merged the two networks (ie. calculated the union), and labelled each node according to whether it was found in the MEG network, the fMRI network, or both (i.e. the overlap, or intersection). As a comparison, the Jaccard coefficient was calculated for cost-matched random networks and the mean and standard deviation of

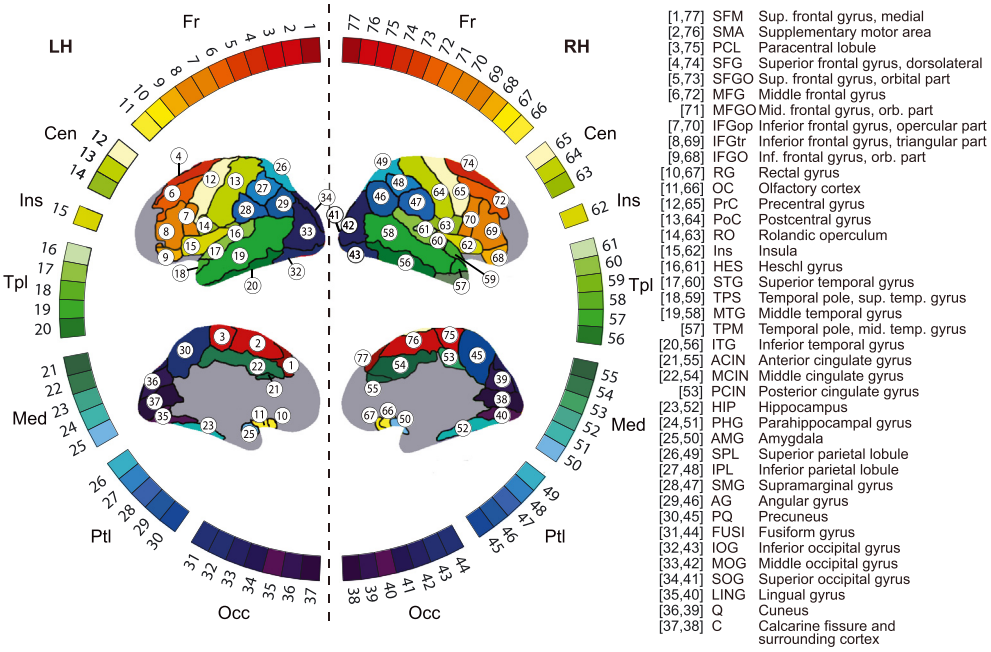

Fig. 1. Visualization of the adjacency matrix in a circular diagram. Coloured squares along the circle represent brain regions, parcellated according to the AAL (Tzourizio-Mazoyer et al., 2002) anatomical labelling scheme, and annotated accordingly. The surface image shows a schematic view of the anatomical regions (not all regions are visible on the surface). LH — left hemisphere, RH — right hemisphere, Fr — Frontal lobe, Cen — Central regions, Ins — Insula, Tpl — Temporal lobe, Med — Medial cortex, Ptl — Parietal lobe, Occ — Occipital lobe.

the coefficient over 1000 permutations was computed. Significance of the overlap between the measured MEG and fMRI networks was assessed at costs ranging from 0.01 to 0.1 (in steps of 0.01) using the hypergeometric distribution, which tests for overrepresentation of overlapping edges in the drawn sample (e.g. Fuxman Bass et al., 2013).

The spatial distribution of average network hub locations was determined by taking the significant ($p < 0.0005$; minimum cluster size 3 for both MEG and fMRI) connectivity data averaged across frequencies at the original grid locations. In concordance with the network overlap criterion specified above, we focused on the high-density connections as those connections are likely to be at the core of the functional networks (Tewarie et al., 2014). The cortical regions falling within the top 20% of connection density were thus rendered on the pial surface. To identify common hub areas between modalities the direct spatial overlap ranging from 5% to 20% (in steps of 5%) of the most connected nodes in MEG and fMRI was calculated. Direct overlap of network nodes was determined for the original grid locations.

Topologically important nodes, such as hubs or bottlenecks can be inferred by graph theoretical measures. In order to quantitatively characterize the MEG and fMRI networks, we applied two widely used network measures, degree and betweenness centrality (Rubinov and Sporns, 2010). The degree of a node reflects the total number of connections to that node, whereas the betweenness centrality of a node is equal to the fraction of the shortest paths between all pairs of nodes that pass through that specific node (Sporns et al., 2007). Graph theoretical measures are dependent on the wiring cost of the network (Achard

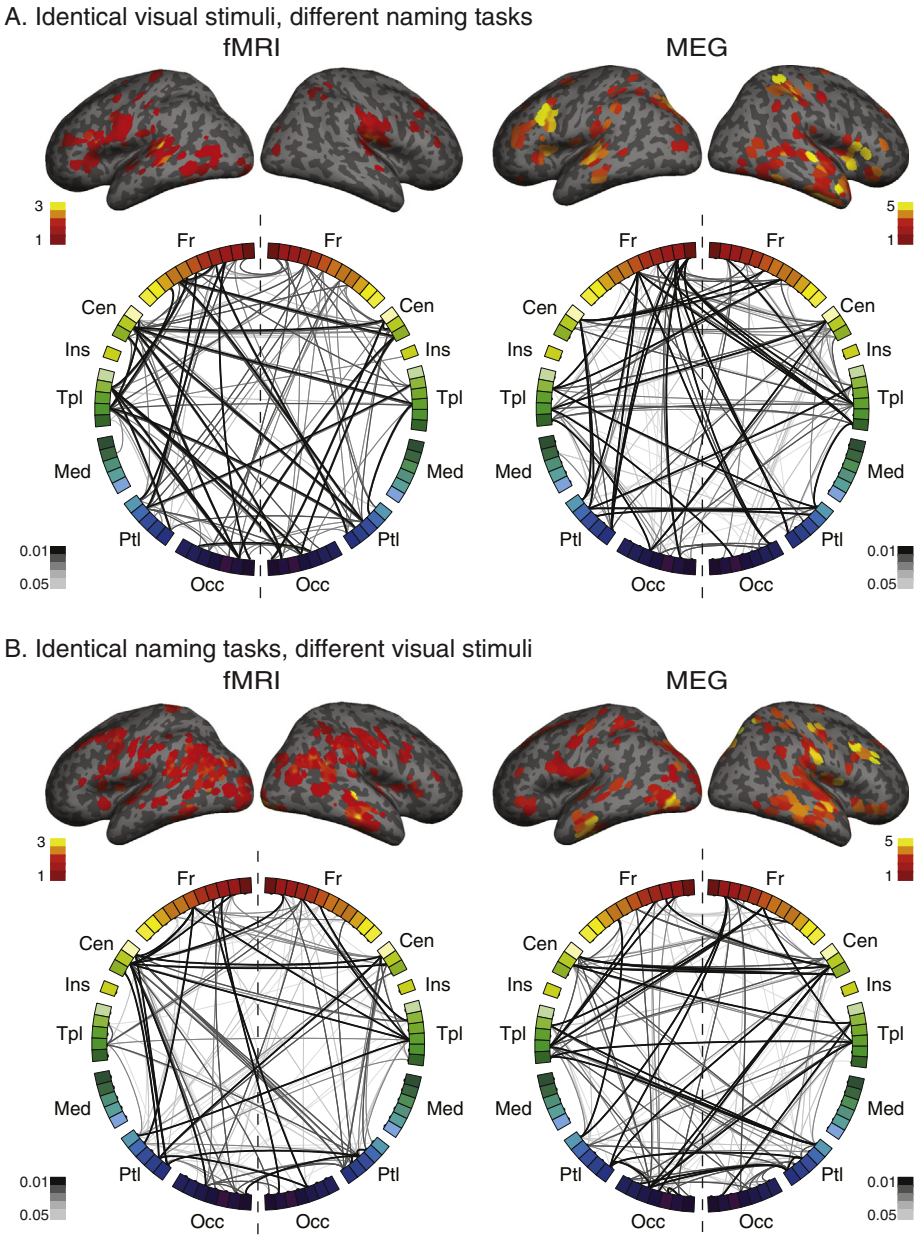

Fig. 2. Network connections illustrated on a circular representation of the cortex at different cost levels. A) Action vs. object naming; identical (action) image, B) Action vs. object images; identical task of object naming. fMRI (*left*) and MEG (*right*) network hubs exhibiting significant ($p < 0.0005$; minimum cluster size 3 for both modalities) task- or stimulus-related connectivity modulations, represented on a normalized pial surface (*above*). Results are averaged across frequency bands. The 20% most connected grid locations are shown. Regions are color-coded according connection density. The associated average network structures are depicted on a circular representation of the cortical surface (*below*). Lines are color-coded according to wiring cost, *K*, ranging from 0.05 (light grey) to 0.01 (black). See Fig. 1 for abbreviations.

and Bullmore, 2007; Ginestet et al., 2011, 2014; van Wijk et al., 2010). To estimate the robustness of the identified hubs at different cost levels we calculated the degree and betweenness centrality at cost levels ranging from 0.01 to 0.1 (in steps of 0.01). The relative importance of each region was evaluated by ranking the regions according to the median of the normalized degree and betweenness centrality across cost levels and visualized using a box-plot. Brain regions with the highest ranking degree and betweenness centrality were defined as central

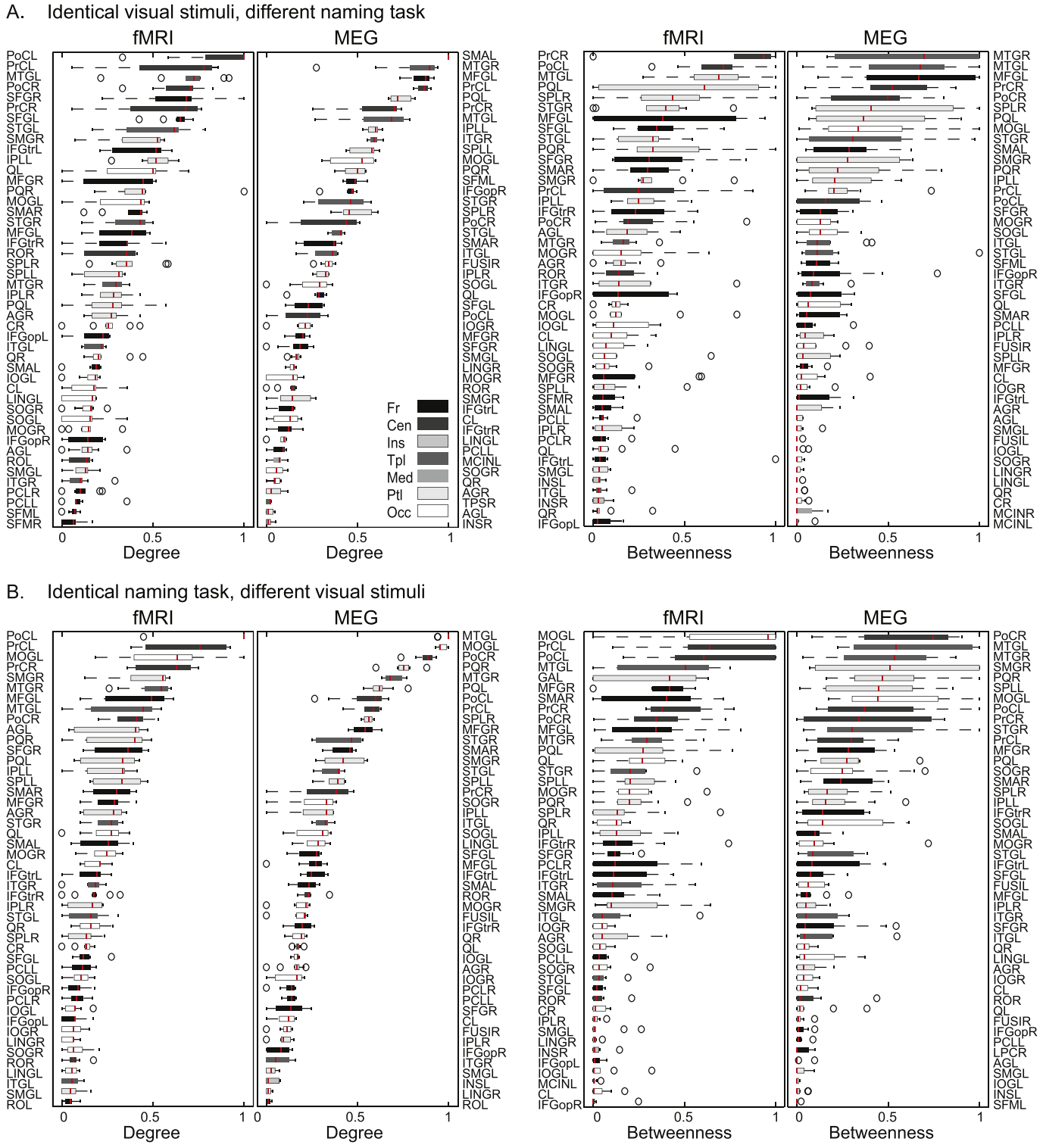

Fig. 3. Degree and betweenness centrality across cost levels. A) Action vs. object naming; identical (action) image, B) Action vs. object images; identical task of object naming. Brain regions are ranked in order of decreasing degree (*left*) and betweenness centrality (*right*). The horizontal line inside each box shows the median value across cost levels ($0.01 < K < 0.1$). Each box spans from the first to the third quartile, and the end of the whiskers show the minimum and maximum values. Outliers are shown as circles. Brain regions with consistently high median value and small interquartile range were identified as hubs. Regions are color-coded according to lobar region, see Fig. 1 for abbreviations for the anatomically parcellated brain regions and the division into lobes. Fr — Frontal lobe, Cen — Central regions, Ins — Insula, Tpl — Temporal lobe, Med — Medial cortex, Ptl — Parietal lobe, Occ — Occipital lobe. L — left hemisphere, R — right hemisphere.

nodes, or hubs. We also estimated the connectivity profile for the highest ranking regions at the lobar level for both MEG- and fMRI-derived networks. For this comparison we chose, for each modality, the two highest ranking lobar regions and calculated (from the lobar adjacency matrices) the percentage of connections between this region and other lobar regions.

To investigate the nature of the relationship between the individual frequency components of the MEG- and fMRI-derived networks, a similarity index (Pearson's correlation coefficient) was computed between each MEG and fMRI adjacency matrix. The similarity indices were plotted as a function of MEG frequency to determine whether a dominant frequency exists which most closely corresponds with the haemodynamic networks. As network topologies may vary in a complex manner with respect to the number and weighting of network connections (Ginestet et al., 2011; van Wijk et al., 2010) we assessed the stability of the MEG–fMRI relationship across a range of network costs. To this end, a more lenient statistical threshold (paired Student's t-test $p < 0.005$, minimum cluster size 3) was used in both modalities. Unweighted adjacency matrices were matched for number of network edges for the cost range $0.1 < K < 0.5$, in steps of 0.1 (see Inline Supplementary Figure S2). This stability analysis was performed for one task comparison (identical visual stimuli, different naming tasks), and one fMRI frequency band (0.001–0.023 Hz). The overall shape of the curve was robust to cost level variations, and based on this analysis (Inline Supplementary Figure S2), the wiring cost was fixed at 0.4 in all further calculations of the similarity index. Differences between cross-spectral curves of the two types of experimental (task- or stimulus-specific) manipulations were assessed using a set of 1000 permutations. The task-specific and stimulus-specific cross-spectral curves were considered to differ when the correlation plus one standard deviation did not overlap.

Inline Supplementary Fig. S2 can be found online at http://dx.doi.org/10.1016/j.neuroimage.2015.07.017.

Results

Identical visual stimuli, different naming tasks

Haemodynamic changes in cortical connectivity

The data driven all-to-all connectivity approach revealed several prominent fMRI average network hubs which were modulated when the participant was required to execute different naming tasks (verb vs. noun naming), while the stimulus remained the same (action image). Fig. 2A *left* illustrates the 20% most connected cortical regions displaying significant ($p < 0.0005$; minimum cluster size 3) task-related modulations in average fMRI connectivity and the underlying network structure, at cost levels ranging from 0.01 to 0.05. Frequency-specific networks are shown in Inline Supplementary Figure S3. The analysis revealed prominent intra-hemispheric connections linking the left temporal cortex with the inferior frontal regions (pars opercularis and pars triangularis), sensorimotor regions and the occipital cortex. In the right hemisphere, sensorimotor and occipital regions were connected. Prominent inter-hemispheric connections were observed between right sensorimotor cortex and frontal regions. Network hubs with high connection density (degree) were observed bilaterally in the sensorimotor (PoC, PrC) and superior frontal cortex (SFG), in the left superior/middle temporal (STG, MTG) and in the inferior frontal

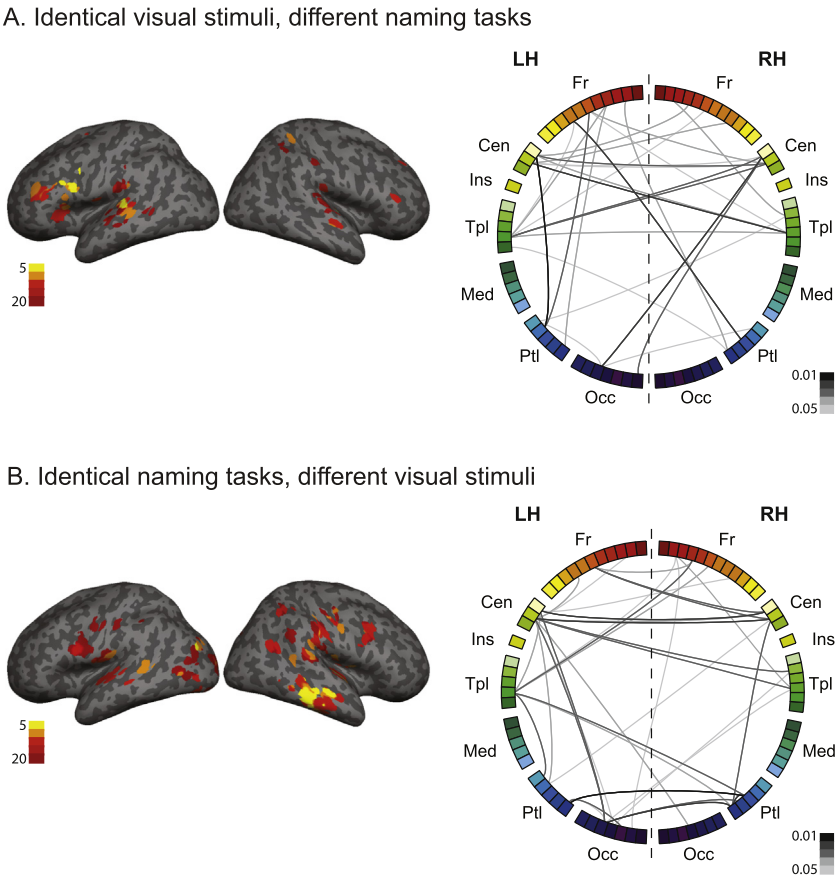

Fig. 4. Correspondence between MEG and fMRI networks. A) Action vs. object naming; identical (action) image, B) Action vs. object images; identical task of object naming. Common MEG and fMRI hub locations (*left*) were defined as directly overlapping regions. Regions are color-coded according to overlap threshold, ranging from overlap at the 20% top connections (red) to overlap at the top 5% connections (yellow). Cortical connections shared between MEG and fMRI are illustrated in a circular connectivity diagram (*right*). Lines between regions demonstrate directly shared connections, and are color-coded according to network cost, ranging from overlap at wiring cost 0.05 (light grey) to 0.01 (black).

cortex (IFG) (Fig. 3A, *left*). In addition, the precuneus (PQ) and the superior parietal lobule (SPL) were identified as central nodes as indicated by high betweenness centrality (Fig. 3A, *right*). Overall, the degree measure was more stable across cost levels than betweenness centrality, as indicated by the smaller interquartile range for degree than for betweenness centrality.

Inline Supplementary Fig. S3 can be found online at http://dx.doi.org/10.1016/j.neuroimage.2015.07.017.

Electrophysiological changes in cortical connectivity

Fig. 2A *right* illustrates the 20% most connected cortical regions and the connectivity network structure of the average MEG network modulations at cost levels ranging from 0.01 to 0.05 when the participant was performing different naming tasks. The frequency-specific networks are shown in Inline Supplementary Figure S4. Within the left hemisphere, pronounced parieto-frontal and temporo-frontal connections were observed. These connections were prominent in the high beta and gamma range (Inline Supplementary Figure S4). Inter-hemispheric connectivity modulations could be observed between left and right sensorimotor and left and right temporal cortices. The left sensorimotor cortex exhibited connectivity modulations involving left inferior parietal and right prefrontal regions. Connections were also observed between the left medial frontal cortex and the precuneus. These modulations were prominent in the low gamma range (Inline Supplementary Figure S4). Salient network hubs appeared in the left supplementary motor area (SMA), middle frontal gyrus (MFG), and precuneus (PQ), and bilaterally in the middle temporal gyrus (MTG), and precentral cortex (PrC) (Fig. 3A *left*). The bilateral middle temporal cortex (MTG), left middle frontal cortex (MFG), and right sensorimotor cortex (PrC, PoC) were central nodes in the network as indicated by betweenness centrality (Fig. 3A *right*).

Inline Supplementary Fig. S4 can be found online at http://dx.doi.org/10.1016/j.neuroimage.2015.07.017.

Haemodynamic vs. electrophysiological connectivity modulations

Cortical hubs common to both modalities when the two naming tasks were contrasted are shown in Fig. 4A *left*. The core regions, identified both in MEG and fMRI network analysis, were the left superior and middle temporal cortices, and the left inferior and middle frontal gyri. Shared edges between the two modalities (Fig. 4A *right*) linked the inferior parietal and the left middle temporal cortex to the left precentral and inferior frontal gyrus. Interhemispheric connections between left and right sensorimotor regions and the left and right middle temporal cortices were observed. The Jaccard coefficient of similarity, plotted across wiring cost levels ranging from 0.01 to 0.1 showed a clear dependency on cost level, with increasing similarity observed for networks depicted at a more lenient threshold (Fig. 5A, *top*). For comparison, the figure also displays the Jaccard coefficient for cost-matched random networks (mean and standard deviation across 1000 permutations). The Jaccard coefficient increased as a function of cost also for random networks, but the effect was not as pronounced as for the overlap between the measured MEG and fMRI networks. The overlap between the networks was significant for cost levels $K > 0.03$ (Fig. 5A, *bottom*).

For a compact view of the most common connections we calculated the degree at the lobar level (Inline Supplementary Figure S5A) and focused on the MEG and fMRI connectivity profiles for lobar regions with the highest ranking in either the MEG or fMRI networks. At the lobar level, the left frontal cortex ranked high in both MEG and fMRI (Inline Supplementary Figure S5A). In MEG, connections in the left frontal cortex were mostly with the parietal (left: 24%, right: 16% of all connections from this region, calculated as the mean over cost levels ranging from 0.01 to 0.1), and the right temporal (21%) lobes. Similarly, in fMRI, connections were observed between the left frontal lobe and the parietal (right: 17%, left: 16%) and left temporal (14%) lobes. A dominant cortical hub was found with MEG in the left parietal lobe (Inline Supplementary Figure S5A). In MEG, most connections from the left parietal lobe were

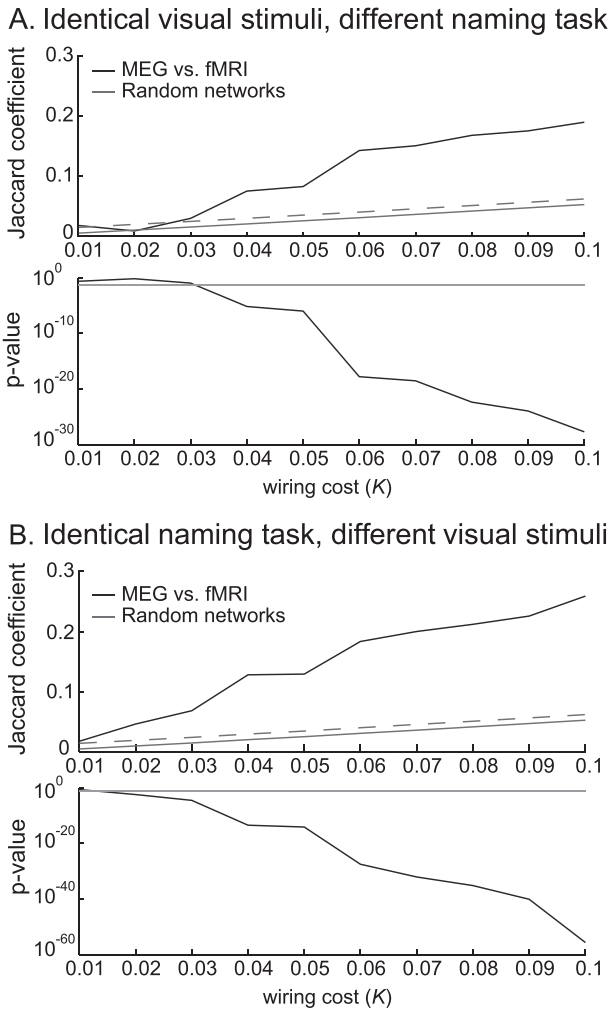

Fig. 5. Jaccard coefficient and significance of overlap between MEG and fMRI networks for cost levels $0.01 < K < 0.1$. The Jaccard coefficient (*top*) gives the fraction of overlapping edges as compared to the union of edges in the two networks. For comparison, the Jaccard coefficient for overlap between cost-matched random networks is shown (grey lines, mean and standard deviation over 1000 permutations). Significance of overlap (*bottom*) was assessed at each cost level using the hypergeometric distribution which tests for over-representation of overlapping edges. The 0.05 significance level is shown in grey.

with the left frontal cortex (32%), the left sensorimotor cortex (21%), and right parietal cortex (20%). In fMRI, the left parietal lobe was connected with the bilateral frontal (left: 24%, right: 17%) and the left occipital cortex (13%). In fMRI, the right frontal cortex was also strongly represented (Inline Supplementary Figure S5A). Most fMRI connections in the right frontal cortex were with the left temporal cortex (14%), the right parietal cortex (14%), and between regions within the right frontal cortex (14%). In MEG, most connections from the right frontal cortex were with the left sensorimotor cortex (26%), and the temporal cortex (right: 24%, left: 17%).

Inline Supplementary Fig. S5 can be found online at http://dx.doi.org/10.1016/j.neuroimage.2015.07.017.

Identical naming tasks, different visual stimuli

Haemodynamic changes in cortical connectivity

Fig. 2B *left* shows the average fMRI network exhibiting modulation in coherence, when the subject was performing the same task (object naming) but was presented with different visual stimuli (action vs. object image), rendered on the cortical surface with the underlying connection structure shown below. A dominant centro-parietal network was evident in the network structure alongside prominent connections

between left occipital cortex and the parietal and sensorimotor cortex. In addition, the right middle temporal gyrus showed strong connections with bilateral parietal and sensorimotor regions. Network hubs were observed bilaterally in the sensorimotor regions (PoC, PrC), in the left middle occipital cortex (MOG) and middle frontal gyrus (MFG), and in the right supramarginal (SMG) and middle temporal gyrus (MTG) (Fig. 3B *left*). Nodes that were central to the network, as indicated by betweenness centrality (Fig. 3B *right*), were observed in the left hemisphere in the middle occipital cortex (MOG), the sensorimotor cortex (PrC, PoC) and the middle temporal and angular gyri (MTG, AG).

Electrophysiological changes in cortical connectivity

Fig. 2B *right* illustrates how the average MEG-derived networks were modulated when the subject was required to undertake a constant task but was presented with different visual stimuli, i.e. object naming from either action or object pictures. Prominent connections were seen between the occipital and temporal cortices, with additional connections between the left occipital lobe and bilateral precuneus and sensorimotor regions. Inter-hemispheric connections were observed between the sensorimotor regions. Network hubs were observed in the left middle occipital cortex (MOG), and bilaterally in middle temporal cortex (MTG), the precuneus (PQ) and the sensorimotor cortex (PoC, PrC) (Fig. 3B *left*). Central nodes were found in the middle temporal cortex (MTG) bilaterally, in the right postcentral gyrus (PoC) and the precuneus (PQ), as shown by betweenness centrality (Fig. 3B *right*).

Haemodynamic vs. electrophysiological connectivity modulations

Cortical hubs common to both modalities when stimulus content was manipulated (action image vs. object image) are shown in Fig. 4B *left* and included, bilaterally, the middle occipital gyri, middle temporal gyri and sensorimotor cortices. Fig. 4B *right* shows the directly shared connections at different cost levels: the right sensorimotor cortex was linked with several other intra- and interhemispheric regions (left sensorimotor, frontal and occipital; right temporal and parietal), and the left occipital cortex was connected with both bilateral parietal and left sensorimotor cortices. The Jaccard coefficient of similarity reached higher values for the comparison between different visual stimuli than for the comparison between different naming tasks (Fig. 5). The overlap between the MEG and fMRI networks increased with cost level, and was significant for cost levels $K > 0.01$ (Fig. 5B, *bottom*).

To investigate whether the manner in which the connections were modulated by stimuli were comparable across different modalities we focused on the main connections of the lobar regions that ranked highest in either MEG or fMRI. At the lobar level, the MEG-derived network (Inline Supplementary Figure S5B, *right*) revealed a prominent network hub in the left occipital lobe. Notably, the left middle occipital cortex (MTG) ranked high in degree (Fig. 3B, *left*) and betweenness (Fig. 3B, *right*) in both fMRI and MEG for the condition when different images were contrasted. At the lobar level, MEG connections for the left occipital cortex were mostly with the right parietal (20% of all connections from this region), right temporal (19%), and left parietal (14%) lobes. fMRI connections between the left occipital cortex and other lobar regions were with the left sensorimotor cortex (27%), right parietal lobe (19%) and right frontal lobe (13%). Both MEG- and fMRI-derived networks displayed connectivity modulations in the right parietal lobe. In MEG most connections from the right parietal lobe were with the left temporal cortex (24%), the left occipital (21%), and other regions within the right parietal lobe (16%). In fMRI, most connections were within the parietal lobe (20%), with the left occipital lobe (20%), and the right sensorimotor cortex (12%). The left sensorimotor cortex was ranked high in lobar degree in the fMRI-derived network (Inline Supplementary Figure S5B). Here, most connections were with other regions within the left sensorimotor cortex (17%), the left occipital cortex (16%), and the left frontal lobe (12%). In MEG, the left sensorimotor cortex did, overall, not rank as high as in fMRI (Inline Supplementary Figure S5B), and most connections were with the right sensorimotor (41%) cortex.

Frequency-specificity of the observed networks

Fig. 6A demonstrates the cross-spectral correlation between fMRI- and MEG-derived oscillatory networks modulated by naming task (action vs. object naming; identical stimulus). For all fMRI frequencies, correlation with MEG frequencies revealed salient peaks in the alpha and low-beta frequencies (7–13 Hz and 13–17 Hz), with the dominant peak in the 13–17 Hz frequency range (correlation 0.27–0.3). In the lower gamma bands the correlation was weakest, with an increase in correlation coefficient for the high gamma band (>60 Hz) for the fMRI frequencies 0.001–0.023 Hz and 0.11–0.14 Hz. Fig. 6B demonstrates the cross-spectral correlation between MEG- and fMRI-derived oscillatory networks modulated by different visual images (depicting actions vs. objects only; identical naming task). The strongest correlation with MEG data (correlation 0.27) occurred in the low-frequency range with the peak centred at 3–7 Hz (theta band). Other peaks were observed at 13–17 Hz (low beta) and 52–60 Hz (high gamma).

The comparison between the cross-spectral curves for the task-specific vs. stimulus-specific correlations is depicted in Fig. 6C, separately for each fMRI frequency. Differences between the task-specific and stimulus-specific cross-spectra were observed at multiple MEG frequency ranges (3–7 Hz, 13–17 Hz, 17–25 Hz, and 52–60 Hz), depicting a shift in network structure when moving from a task-dependent to a stimulus-dependent modulation. While the cross-spectral correlation trends were similar across fMRI frequencies (Fig. 6A), some differences between the fMRI frequency bands were also observed (Inline Supplementary Figure S6).

Inline Supplementary Fig. S6 can be found online at http://dx.doi.org/10.1016/j.neuroimage.2015.07.017.

Discussion

Using a data driven approach to functional connectivity in a parallel MEG/fMRI picture naming study, we investigated the similarities between haemodynamic networks and their electrophysiological counterparts. This study demonstrates similarities, but also found discrepancies, in the spatial distribution of functionally relevant network hubs identified using data from MEG and fMRI. Overall, the study suggested a differentiation in the MEG–fMRI large-scale patterns underlying task-driven vs. stimulus-driven network modulations. This differentiation was also observed in the frequency-specificity of the identified networks.

Task- and stimulus-driven modulations in MEG- and fMRI-derived functional networks

When action and object naming from the same set of images were contrasted, spatial correspondence between MEG and fMRI network hubs was seen in cortical regions that have been previously reported to be strongly implicated in language production. Network hubs in the perisylvian regions (middle temporal gyrus, inferior frontal gyrus, inferior parietal cortex) and the sensorimotor cortex were consistently modulated in both MEG and fMRI. These hub loci are in line with strongly activated sites reported in numerous studies that have employed picture naming tasks: left inferior and middle frontal gyrus, the left posterior middle temporal gyrus and left parietal areas (Hultén et al., 2014; Indefrey and Levelt, 2004; Price, 2012; Roskies et al., 2001; Salmelin et al., 1994). Furthermore, the directly shared cortico-cortical connections between the left temporal/inferior parietal and inferior/middle frontal regions are in good agreement with structural connectivity (Catani et al., 2005): the arcuate fasciculus is a white matter tract which provides a direct pathway between temporal and frontal regions and includes an indirect segment involving inferior parietal regions. Importantly, the arcuate fasciculus has also been viewed as the critical white matter pathway to provide the scaffolding for the language network (Catani and Mesulam, 2008).

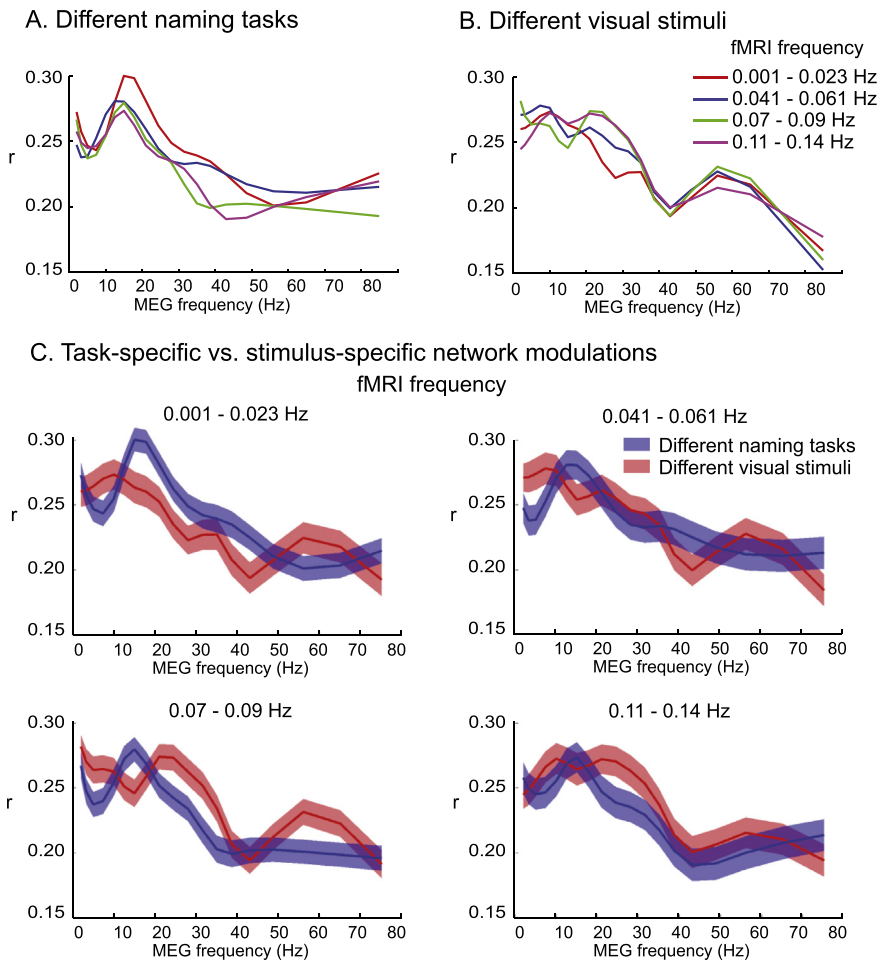

Fig. 6. Cross-spectral similarity between MEG and fMRI unweighted network topologies. A) Action vs. object naming; identical stimulus (action image), B) Action vs. object images; identical task of object naming. Correlation between MEG and fMRI networks is plotted as a function of MEG frequency, with separate curves for the various tested fMRI frequencies. C) Task-related vs. stimulus-related cross-spectral similarity. At each fMRI frequency the overlap between the cross-spectral curves between task- and stimulus-specific manipulations was assessed. Variation in the cross-spectral correlation was estimated by randomly permuting the connections for each manipulation. The task-specific and stimulus-specific cross-spectral curves were considered to differ when the correlation plus one standard deviation did not overlap. All correlations are significant at $p < 10^{-12}$ (Bonferroni corrected).

When contrasting action and object images, while keeping the task constant, the observed connectivity pattern was notably different. Both MEG and fMRI networks exhibited extensive modulations in brain wide connectivity, but the overlapping MEG–fMRI network hubs were predominantly found in the lateral occipital cortices (particularly in the left hemisphere), middle temporal and sensorimotor regions. The lateral occipital cortex is critical for visual processing and object recognition (Grill-Spector et al., 2001) and an increased contribution in this region is in concordance with differences in visual content of the action vs. object images. A clear difference between the MEG- and fMRI-derived networks was, however, observed in the connectivity pattern of the lateral occipital cortex. A large proportion of the MEG-derived network connections were observed between the occipital cortex and the temporo-parietal cortices whereas the occipital lobe connections in the fMRI-derived network were largely with parieto-frontal regions. The temporal lobes have been implicated in the human ventral visual pathway involved in visual and language processing (Ishai et al., 1999), while the parieto-frontal network is involved with the spatial aspects of attention and in sustaining attention (Malhotra et al., 2009). The distinction in the connection patterns suggests a functional divergence in the roles of the networks identified with haemodynamic and electrophysiological measures, with the network identified with MEG inclined towards a more bottom-up role of stimulus processing and the network revealed with fMRI reflecting a top-down role in modulating selective attention. This illustrates that although the same cortical regions may appear in networks derived from MEG and fMRI, the manner in which these cortical regions are integrated into the network and their hierarchical position within the network is not necessarily the same.

Frequency dependence of the MEG–fMRI networks

Haemodynamic signals typically show a frequency-dependent relationship with electrophysiological effects, often exhibiting negative correlations for low (<30 Hz) and positive correlations for high (>30 Hz) frequency activity (Mukamel et al., 2005). This relationship is, however, location-specific and may depend on factors such as local cytoarchitecture (Ekström et al., 2009; Kujala et al., 2014).

Here, the greatest similarity between MEG and fMRI derived networks was observed at neural frequencies below 30 Hz. The dominant electrophysiological oscillatory frequencies underpinning the haemodynamic networks that we report thus fall in the same alpha to beta frequency range (8–25 Hz) that has been identified as the dominant band of carrier frequencies in spontaneous electrophysiological networks (Brookes et al., 2011a; de Pasquale et al., 2012; Hipp et al., 2012). Such low frequency oscillatory activity has been purported to be the key mechanism for long-range neuronal interaction and information transfer (Donner and Siegel, 2011; Kopell et al., 2000). Our results further suggest that gamma frequency band interactions contribute to the haemodynamic networks.

Remarkably different spectral profiles of MEG–fMRI network correspondence were observed for the task-driven vs. stimulus-driven connectivity modulations. Haemodynamic network interactions thus cannot be attributed to a single frequency band, but the entire spectral profile should be taken into account when assessing the correspondence between MEG and fMRI networks. Although the structure of the low frequency MEG networks most closely resembles the haemodynamic networks and similarities can be found between hub locations in the two modalities, divergences in spectral similarity between tasks illustrate the complexity of the relationship between haemodynamics and electrophysiology.

Relationship to resting state networks

Several of the network hubs found here in left perisylvian language regions when contrasting naming tasks often appear as a network of correlated regions in resting-state fMRI analyses, including the left inferior frontal, posterior temporal and inferior parietal cortices (Tomasi and Volkow, 2012; Xiang et al., 2010). The convergent MEG and fMRI connectivity in the left middle temporal gyrus is also in line with previous structural and functional resting state connectivity studies (Binder et al., 2009; Turken and Dronkers, 2011), which propose the left middle temporal gyrus to be a focal point for the language network due to its richness of connections. Previous studies have demonstrated an overlap between network hubs identified from resting state fMRI data and cortical regions implicated in task by activation studies (Smith et al., 2009). Here we found commonalities in network hubs derived from a linguistic task dataset and those commonly seen in seed-based fMRI resting state studies using the left middle temporal gyrus (Turken and Dronkers, 2011) or the left inferior frontal cortex (Xiang et al., 2010) as a seed.

The task network data reported in the current study show involvement of additional cortical regions, e.g. right sensorimotor cortex. This area is typically thought to belong to an independent resting state network in the sensorimotor cortex and yet here shows direct connections to the left middle temporal gyrus. This is in line with a recent study by (Gonzalez-Castillo et al., 2012) which reported that right motor cortex and higher order visual areas (e.g. the medio-temporal area), usually attributed to well differentiated resting state networks, were assigned to the same cluster in a task network. Findings such as these demonstrate the need to interrogate task-related connectivity networks in detail since resting-state networks, although not completely disrupted by task, clearly undergo some specific reorganization to facilitate task performance.

Methodological considerations

Topological properties of a network depend on the number of nodes in the network, and the number of connections among those nodes. We therefore used an approach that matched both the grid space and the number of connections within the networks (wiring cost) across MEG and fMRI. Thresholding is critical when comparing networks. A strict threshold will produce sparse networks with low cost, but similarities in the underlying network structure may go undetected. At high cost, networks are more likely to overlap (Achard and Bullmore, 2007; Ginestet et al., 2011), but with a lenient threshold some edges may be spurious. We assessed network overlap at multiple cost levels and observed increasing similarity between MEG and fMRI for networks with a higher wiring cost. Moreover, the similarity increased more than for cost-matched random networks. At a very strict threshold the overlap was not statistically significant. Our results illustrate the benefit of assessing network similarity at multiple cost levels; while individual edges may be spurious at low thresholds and should be viewed with some caution, we were able to show that the general overlap between the MEG and fMRI networks is much higher than expected by chance.

To identify cortex-wide connectivity patterns we used coherence as a metric for connectivity in both MEG and fMRI. Coherence is a neurophysiologically well-motivated measure for MEG-derived connectivity (Fries et al., 2005). In addition, coherence-based connectivity mapping of MEG signals allows for direct whole-cortex mapping of connectivity at different frequencies using a beamformer without the need to estimate time series at the level of cortical sources (Gross et al., 2001; Kujala et al., 2008; Liljeström et al., 2015). This is an advantage since time series distortions have been observed when using beamformers to reconstruct source time courses in data sets with high correlations between sources (Huang et al., 2014).

In a beamformer approach, a spatial filter is optimized to pass activity from a certain brain region at unit gain while suppressing activity from all other areas (van Veen et al., 1997). To achieve such suppression, the assumption is that the other sources are not correlated with the target location. While brain regions commonly display correlated activity, the correlations between them are normally lower than would be needed to markedly affect the beamforming suppression (Gross et al., 2001; Hadjipapas et al., 2005; Hillebrand et al., 2005). Beamformer source detection can, however, be difficult when the sources are highly correlated (e.g. $r > 0.5$, Hillebrand et al., 2005; Hadjipapas et al., 2005; Huang et al., 2014). This could be the case for low-level evoked responses that are averaged with respect to stimulus presentation. Here, responses were not averaged with respect to the task onset, and in a complex cognitive task the correlation between sources is likely to be lower than in simple motor or visual tasks.

Due to the inherent spatial smoothing of the MEG signal, field spread must be taken into account in MEG connectivity analysis. To alleviate effects of spurious connectivity we used a power-matched control condition and estimated connectivity differences between conditions. In this approach, we test for power differences at every sensor, thus controlling that the spatial pattern of active cortical regions, and their source power, are essentially the same in both conditions. Field spread effects are highly dependent on the amplitude of the measured sources, and by using power-matched conditions we thus make the assumption that these effects are identical across conditions and therefore cancel out (Kujala et al., 2007, 2008; Gross et al., 2013a; Schoffelen and Gross, 2009). Since this assumption may not be completely fulfilled at each location, we additionally used a minimum distance limit between source regions (similarly to de Pasquale et al., 2012; Kujala et al., 2008; Liljeström et al., 2015). We have recently used this approach in identifying large-scale cortical networks underlying motor performance, auditory processing, visual recognition (Saarinen et al., 2015), and language production (Liljeström et al., 2015). Important in this context is, however, that the resulting networks reflect task-related, long-range modulations in connectivity, rather than the entire underlying network. Another approach would be to use a measure of connectivity that is less sensitive to field spread. Such measures can be crucial for obtaining reliable estimates of connectivity from resting-state data (Hipp et al., 2012; Hillebrand et al., 2012; Brookes et al., 2011a). One such measure that could be applied to both MEG and fMRI data is imaginary coherence. However, using imaginary coherence can be problematic when comparing two conditions, as interpreting changes between conditions in the imaginary part of the coherence is not straightforward (e.g. Gross et al., 2013a).

Some differences between the networks identified from MEG and fMRI data can be explained by possible limitations in the currently available data acquisition and analysis techniques. In fMRI, cardiac and respiratory fluctuations are known to manifest themselves in the form of spatially and temporally structured noise (Birn et al., 2006). Efforts were made in this study to minimise the contributions from physiological effects (time-courses from regions thought to exhibit non-neuronal fluctuations were regressed out (Behzadi et al., 2007) and motion parameters accounted for), however, it is impossible to completely rule out their contributions. In addition, there may be other non-neuronal or vascular changes that could give rise to modulations in oscillatory activity (e.g., arterial blood pressure is also known to vary at ~0.1Hz (Katura et al., 2006)).

Conclusions

In this work we have examined the relationship between task-related functional connectivity networks as detectable by MEG and by fMRI. Connectivity analysis revealed network hubs in cortical regions previously associated in activation studies with language processing, object recognition and visual processing; these hubs were evident in both modalities. The highest correlation between electrophysiological and haemodynamic networks was demonstrated at neural frequencies below 30 Hz, consistent with resting-state studies. The direct overlap of functionally relevant areas, independently elicited by two disparate modalities adds weight to the argument that haemodynamic networks are, at least partially, supported by electrophysiological counterparts (Brookes et al., 2011b). In addition, we observed a striking difference in functional connectivity between tasks manipulations. Overall, the results depict a shift in network structure when moving from a task dependent modulation to a stimulus dependent modulation, revealing a reorganization of the large-scale functional connectivity during task performance. Despite similarities, discrepancies between the two modalities were observed both in terms of key network hubs and network connection structure. This provokes further questions both as to the functional role of the respective networks and the nature of their relationship during task execution.

Acknowledgments

This work was supported by the Academy of Finland (National Centres of Excellence Programme 2006–2011,LASTU Programme 2012–2016, personal grants to JK and RS), Sigrid Jusélius Foundation, Finnish Cultural Foundation, Swedish Cultural Foundation in Finland, Brain Research at Aalto University and University of Helsinki (BRAHE)-consortium, and the Finnish Funding Agency for Technology and Innovation (SalWe Strategic Center for Science, Technology and Innovation in Health and Well-being).

References

Achard, S., Bullmore, E., 2007. Efficiency and cost of economical brain functional networks. PLoS Comput. Biol. 3, e17.
Achard, S., Salvador, R., Whitcher, B., Suckling, J., Bullmore, E., 2006. A resilient, low-frequency, small-world human brain functional network with highly connected association cortical hubs. J. Neurosci. 26, 63–72.
Arbabshirani, M.R., Havlicek, M., Kiehl, K.A., Pearlson, G.D., Calhoun, V.D., 2013. Functional network connectivity during rest and task conditions: a comparative study. Hum. Brain Mapp. 34, 2959–2971.
Behzadi, Y., Restom, K., Liau, J., Liu, T.T., 2007. A component based noise correction method (CompCor) for BOLD and perfusion based fMRI. NeuroImage 37, 90–101.
Betti, V., Della Penna, S., de Pasquale, F., Mantini, D., Marzetti, L., Romani, G.L., Corbetta, M., 2013. Natural scenes viewing alters the dynamics of functional connectivity in the human brain. Neuron 79, 782–797.
Binder, J.R., Desai, R.H., Graves, W.W., Conant, L.L., 2009. Where is the semantic system? A critical review and meta-analysis of 120 functional neuroimaging studies. Cereb. Cortex 19, 2767–2796.
Birn, R.M., Diamond, J.B., Smith, M.A., Bandettini, P.A., 2006. Separating respiratory-variation-related fluctuations from neuronal-activity-related fluctuations in fMRI. NeuroImage 31, 1536–1548.
Biswal, B., Yetkin, F.Z., Haughton, V.M., Hyde, J.S., 1995. Functional connectivity in the motor cortex of resting human brain using echo-planar MRI. Magn. Reson. Med. 34, 537–541.
Brookes, M.J., Gibson, A.M., Hall, S.D., Furlong, P.L., Barnes, G.R., Hillebrand, A., Singh, K.D., Holliday, I.E., Francis, S.T., Morris, P.G., 2005. GLM-beamformer method demonstrates stationary field, alpha ERD and gamma ERS co-localisation with fMRI BOLD response in visual cortex. NeuroImage 26, 302–308.
Brookes, M., Hale, J., Zumer, J., Stevenson, C., Francis, S., Barnes, G., Owen, J., Morris, P., Nagarajan, S., 2011a. Measuring functional connectivity using MEG: Methodology and comparison with fcMRI. NeuroImage 56, 1082–1104.
Brookes, M.J., Woolrich, M., Luckhoo, H., Price, D., Hale, J.R., Stephenson, M.C., Barnes, G.R., Smith, S.M., Morris, P.G., 2011b. Investigating the electrophysiological basis of resting state networks using magnetoencephalography. Proc. Natl. Acad. Sci. U. S. A. 108, 16783–16788.
Buffalo, E.A., Fries, P., Landman, R., Buschman, T.J., Desimone, R., 2011. Laminar differences in gamma and alpha coherence in the ventral stream. Proc. Natl. Acad. Sci. U. S. A. 108, 11262–11267.
Catani, M., Mesulam, M., 2008. The arcuate fasciculus and the disconnection theme in language and aphasia: history and current state. Cortex 44, 953–961.
Catani, M., Jones, D.K., ffytche, D.H., 2005. Perisylvian language networks of the human brain. Ann. Neurol. 57, 8–16.
Cohen, D., 1968. Magnetoencephalography: evidence of magnetic fields produced by alpha-rhythm currents. Science 161, 784–786.
Conner, C.R., Ellmore, T.M., Pieters, T.A., DiSano, M.A., Tandon, N., 2011. Variability of the relationship between electrophysiology and BOLD-fMRI across cortical regions in humans. J. Neurosci. 31, 12855–12865.
de Pasquale, F., Della Penna, S., Snyder, A.Z., Lewis, C., Mantini, D., Marzetti, L., Belardinelli, P., Ciancetta, L., Pizzella, V., Romani, G.L., Corbetta, M., 2010. Temporal dynamics of spontaneous MEG activity in brain networks. Proc. Natl. Acad. Sci. U. S. A. 107, 6040–6045.
de Pasquale, F., Della Penna, S., Snyder, A.Z., Marzetti, L., Pizzella, V., Romani, G.L., Corbetta, M., 2012. A cortical core for dynamic integration of functional networks in the resting human brain. Neuron 74, 753–764.
Donner, T.H., Siegel, M., 2011. A framework for local cortical oscillation patterns. Trends Cogn. Sci. 15, 191–199.
Ekström, A., Suthana, N., Millett, D., Fried, I., Bookheimer, S., 2009. Correlation between BOLD fMRI and theta-band local field potentials in the human hippocampal area. J. Neurophysiol. 101, 2668–2678.
Engel, A.K., Fries, P., Konig, P., Brecht, M., Singer, W., 1999. Temporal binding, binocular rivalry, and consciousness. Conscious. Cogn. 8, 128–151.
Fox, M.D., Raichle, M.E., 2007. Spontaneous fluctuations in brain activity observed with functional magnetic resonance imaging. Nat. Rev. Neurosci. 8, 700–711.
Fries, P., 2005. A mechanism for cognitive dynamics: neuronal communication through neuronal coherence. Trends Cogn. Sci. 9, 474–480.
Fuxman Bass, J.I., Diallo, A., Nelson, J., Soto, J.M., Myers, C.L., Walhout, A.J.M., 2013. Using networks to measure similarity between genes: association index selection. Nat. Methods 10, 1169–1176.
Ginestet, C.E., Nichols, T.E., Bullmore, E.T., Simmons, A., 2011. Brain network analysis: separating cost from topology using cost-integration. PLoS One 6, e21570.
Ginestet, C.E., Fournel, A.P., Simmons, A., 2014. Statistical network analysis for functional MRI: summary networks and group comparisons. Front. Comput. Neurosci. 8.
Gonzalez-Castillo, J., Saad, Z.S., Handwerker, D.A., Inati, S.J., Brenowitz, N., Bandettini, P.A., 2012. Whole-brain, time-locked activation with simple tasks revealed using massive averaging and model-free analysis. Proc. Natl. Acad. Sci. U. S. A. 109, 5487–5492.
Grill-Spector, K., Kourtzi, Z., Kanwisher, N., 2001. The lateral occipital complex and its role in object recognition. Vis. Res. 41, 1409–1422.
Gross, J., Kujala, J., Hämäläinen, M., Timmermann, L., Schnitzler, A., Salmelin, R., 2001. Dynamic imaging of coherent sources: Studying neural interactions in the human brain. Proc. Natl. Acad. Sci. U. S. A. 98, 694–699.
Gross, J., Baillet, S., Barnes, G.R., Henson, R.N., Hillebrand, A., Jensen, O., Jerbi, K., Litvak, V., Maess, B., Oostenveld, R., Parkkonen, L., Taylor, J.R., van Wassenhove, V., Wibral, M., Schoffelen, J.M., 2013a. Good practice for conducting and reporting MEG research. NeuroImage 65, 349–363.
Gross, J., Hoogenboom, N., Thut, G., Schyns, P., Panzeri, S., Belin, P., Garrod, S., 2013b. Speech rhythms and multiplexed oscillatory sensory coding in the human brain. PLoS Biol. 11, e1001752.
Hadjipapas, A., Hillebrand, A., Holliday, I.E., Singh, K.D., Barnes, G.R., 2005. Assessing interactions of linear and nonlinear neuronal sources using MEG beamformers: a proof of concept. Clin. Neurophysiol. 116, 1300–1313.
Hämäläinen, M., Hari, R., Ilmoniemi, R.J., Knuutila, J., Lounasmaa, O.V., 1993. Magnetoencephalography—theory, instrumentation, and applications to noninvasive studies of the working human brain. Rev. Mod. Phys. 65, 413–497.
Hillebrand, A., Singh, K.D., Holliday, I.E., Furlong, P.L., Barnes, G.R., 2005. A new approach to neuroimaging with magnetoencephalography. Hum. Brain Mapp. 25, 199–211.
Hillebrand, A., Barnes, G.R., Bosboom, J.L., Berendse, H.W., Stam, C.J., 2012. Frequency-dependent functional connectivity within resting-state networks: an atlas-based MEG beamformer solution. NeuroImage 59, 3909–3921.
Hipp, J.F., Hawellek, D.J., Corbetta, M., Siegel, M., Engel, A.K., 2012. Large-scale cortical correlation structure of spontaneous oscillatory activity. Nat. Neurosci. 15, 884–890.
Huang, M.-X., Huang, C.W., Robb, A., Angeles, A., Nichols, S.L., Baker, D.G., Song, T., Harrington, D.L., Theilmann, R.J., Srinivasan, R., Heister, D., Diwakar, M., Canive, J.M., Edgar, J.C., Chen, Y.H., Ji, Z., Shen, M., El-Gabalawy, F., Levy, M., McLay, R., Webb-Murphy, J., Liu, T.T., Drake, A., Lee, R.R., 2014. MEG source imaging method using fast L1 minimum-norm and its applications to signals with brain noise and human resting-state source amplitude images. NeuroImage 84, 585–604.
Hultén, A., Karvonen, L., Laine, M., Salmelin, R., 2014. Producing speech with a newly learned morphosyntax and vocabulary: an magnetoencephalography study. J. Cogn. Neurosci. 26, 1721–1735.
Hutchison, R.M., Womelsdorf, T., Allen, E.A., Bandettini, P.A., Calhoun, V.D., Corbetta, M., Della Penna, S., Duyn, J.H., Glover, G.H., Gonzalez-Castillo, J., Handwerker, D.A., Keilholz, S., Kiviniemi, V., Leopold, D.A., de Pasquale, F., Sporns, O., Walter, M., Chang, C., 2013. Dynamic functional connectivity: promise, issues, and interpretations. NeuroImage 80, 360–378.
Indefrey, P., Levelt, W.J., 2004. The spatial and temporal signatures of word production components. Cognition 92, 101–144.
Ishai, A., Ungerleider, L.G., Martin, A., Schouten, J.L., Haxby, J.V., 1999. Distributed representation of objects in the human ventral visual pathway. Proc. Natl. Acad. Sci. U. S. A. 96, 9379–9384.
Jensen, O., Bonnefond, M., VanRullen, R., 2012. An oscillatory mechanism for prioritizing salient unattended stimuli. Trends Cogn. Sci. 16, 200–206.
Katura, T., Tanaka, N., Obata, A., Sato, H., Maki, A., 2006. Quantitative evaluation of interrelations between spontaneous low-frequency oscillations in cerebral hemodynamics and systemic cardiovascular dynamics. NeuroImage 31, 1592–1600.
Kopell, N., Ermentrout, G.B., Whittington, M.A., Traub, R.D., 2000. Gamma rhythms and beta rhythms have different synchronization properties. Proc. Natl. Acad. Sci. U. S. A. 97, 1867–1872.

Kujala, J., Pammer, K., Cornelissen, P., Roebroeck, A., Formisano, E., Salmelin, R., 2007. Phase coupling in a cerebro-cerebellar network at 8–13 Hz during reading. Cereb. Cortex 17, 1476–1485.
Kujala, J., Gross, J., Salmelin, R., 2008. Localization of correlated network activity at the cortical level with MEG. NeuroImage 39, 1706–1720.
Kujala, J., Sudre, G., Vartiainen, J., Liljestrom, M., Mitchell, T., Salmelin, R., 2014. Multivariate analysis of correlation between electrophysiological and hemodynamic responses during cognitive processing. NeuroImage 92, 207–216.
Laaksonen, H., Kujala, J., Salmelin, R., 2008. A method for spatiotemporal mapping of event-related modulation of cortical rhythmic activity. NeuroImage 42, 207–217.
Laaksonen, H., Kujala, J., Hultén, A., Liljeström, M., Salmelin, R., 2012. MEG evoked responses and rhythmic activity provide spatiotemporally complementary measures of neural activity in language production. NeuroImage 60, 29–36.
Liljeström, M., Tarkiainen, A., Parviainen, T., Kujala, J., Numminen, J., Hiltunen, J., Laine, M., Salmelin, R., 2008. Perceiving and naming actions and objects. NeuroImage 41, 1132–1141.
Liljeström, M., Hultén, A., Parkkonen, L., Salmelin, R., 2009. Comparing MEG and fMRI views to naming actions and objects. Hum. Brain Mapp. 30, 1845–1856.
Liljeström, M., Kujala, J., Stevenson, C., Salmelin, R., 2015. Dynamic reconfiguration of the language network preceding onset of speech in picture naming. Hum. Brain Mapp. 36, 1202–1216.
Logothetis, N.K., Pauls, J., Augath, M., Trinath, T., Oeltermann, A., 2001. Neurophysiological investigation of the basis of the fMRI signal. Nature 412, 150–157.
Lohmann, G., Margulies, D.S., Horstmann, A., Pleger, B., Lepsien, J., Goldhahn, D., Schloegl, H., Stumvoll, M., Villringer, A., Turner, R., 2010. Eigenvector centrality mapping for analyzing connectivity patterns in fMRI data of the human brain. PLoS One 5, e10232.
Malhotra, P., Coulthard, E.J., Husain, M., 2009. Role of right posterior parietal cortex in maintaining attention to spatial locations over time. Brain 132, 645–660.
Mantini, D., Perrucci, M.G., Del Gratta, C., Romani, G.L., Corbetta, M., 2007. Electrophysiological signatures of resting state networks in the human brain. Proc. Natl. Acad. Sci. U. S. A. 104, 13170–13175.
Mesulam, M.M., 1990. Large-scale neurocognitive networks and distributed processing for attention, language, and memory. Ann. Neurol. 28, 597–613.
Mukamel, R., Gelbard, H., Arieli, A., Hasson, U., Fried, I., Malach, R., 2005. Coupling between neuronal firing, field potentials, and FMRI in human auditory cortex. Science 309, 951–954.
Muthukumaraswamy, S.D., Singh, K.D., 2009. Functional decoupling of BOLD and gamma-band amplitudes in human primary visual cortex. Hum. Brain Mapp. 30, 2000–2007.
Ogawa, S., Lee, T.M., Kay, A.R., Tank, D.W., 1990. Brain magnetic resonance imaging with contrast dependent on blood oxygenation. Proc. Natl. Acad. Sci. U. S. A. 87, 9868–9872.
Palva, S., Palva, J.M., 2007. New vistas for alpha-frequency band oscillations. Trends Neurosci. 30, 150–158.
Pfurtscheller, G., Lopes da Silva, F.H., 1999. Event-related EEG/MEG synchronization and desynchronization: basic principles. Clin. Neurophysiol. 110, 1842–1857.
Price, C.J., 2012. A review and synthesis of the first 20 years of PET and fMRI studies of heard speech, spoken language and reading. NeuroImage 62, 816–847.
Rosa, M.J., Kilner, J.M., Penny, W.D., 2011. Bayesian comparison of neurovascular coupling models using EEG-fMRI. PLoS Comput. Biol. 7, e1002070.
Roskies, A.L., Fiez, J.A., Balota, D.A., Raichle, M.E., Petersen, S.E., 2001. Task-dependent modulation of regions in the left inferior frontal cortex during semantic processing. J. Cogn. Neurosci. 13, 829–843.
Rubinov, M., Sporns, O., 2010. Complex network measures of brain connectivity: uses and interpretations. NeuroImage 52, 1059–1069.
Saarinen, T., Jalava, A., Kujala, J., Stevenson, C., Salmelin, R., 2015. Task-sensitive reconfiguration of corticocortical 6–20 Hz oscillatory coherence in naturalistic human performance. Hum. Brain Mapp. 36, 2455–2469.
Salmelin, R., Hari, R., 1994. Characterization of spontaneous MEG rhythms in healthy adults. Electroencephalogr. Clin. Neurophysiol. 91, 237–248.
Salmelin, R., Hari, R., Lounasmaa, O.V., Sams, M., 1994. Dynamics of brain activation during picture naming. Nature 368, 463–465.
Salvador, R., Suckling, J., Schwarzbauer, C., Bullmore, E., 2005. Undirected graphs of frequency-dependent functional connectivity in whole brain networks. Philos. Trans. R. Soc. Lond. B Biol. Sci. 360, 937–946.
Schoffelen, J.M., Gross, J., 2009. Source connectivity analysis with MEG and EEG. Hum. Brain Mapp. 30, 1857–1865.
Smith, S.M., Fox, P.T., Miller, K.L., Glahn, D.C., Fox, P.M., Mackay, C.E., Filippini, N., Watkins, K.E., Toro, R., Laird, A.R., Beckmann, C.F., 2009. Correspondence of the brain's functional architecture during activation and rest. Proc. Natl. Acad. Sci. U. S. A. 106, 13040–13045.
Sporns, O., Honey, C.J., Kotter, R., 2007. Identification and classification of hubs in brain networks. PLoS One 2, e1049.
Stam, C.J., 2004. Functional connectivity patterns of human magnetoencephalographic recordings: a 'small-world' network? Neurosci. Lett. 355, 25–28.
Stevenson, C.M., Wang, F., Brookes, M.J., Zumer, J.M., Francis, S.T., Morris, P.G., 2012. Paired pulse depression in the somatosensory cortex: associations between MEG and BOLD fMRI. NeuroImage 59, 2722–2732.
Sun, F.T., Miller, L.M., D'Esposito, M., 2004. Measuring interregional functional connectivity using coherence and partial coherence analyses of fMRI data. NeuroImage 21, 647–658.
Tal, O., Diwakar, M., Wong, C.W., Olafsson, V., Lee, R., Huang, M.X., Liu, T.T., 2013. Caffeine-induced global reductions in resting-state BOLD connectivity reflect widespread decreases in MEG connectivity. Front. Hum. Neurosci. 7, 63.
Taulu, S., Simola, J., 2006. Spatiotemporal signal space separation method for rejecting nearby interference in MEG measurements. Phys. Med. Biol. 51, 1759–1768.
Tewarie, P., Hillebrand, A., van Dellen, E., Schoonheim, M.M., Barkhof, F., Polman, C.H., Beaulieu, C., Gong, G., van Dijk, B.W., Stam, C.J., 2014. Structural degree predicts functional network connectivity: a multimodal resting-state fMRI and MEG study. NeuroImage 97, 296–307.
Tomasi, D., Volkow, N.D., 2012. Resting functional connectivity of language networks: characterization and reproducibility. Mol. Psychiatry 17, 841–854.
Turken, A.U., Dronkers, N.F., 2011. The neural architecture of the language comprehension network: converging evidence from lesion and connectivity analyses. Front. Syst. Neurosci. 5, 1.
Tzourio-Mazoyer, N., Landeau, B., Papathanassiou, D., Crivello, F., Etard, O., Delcroix, N., Mazoyer, B., Joliot, M., 2002. Automated anatomical labeling of activations in SPM using a macroscopic anatomical parcellation of the MNI MRI single-subject brain. NeuroImage 15, 273–289.
van den Heuvel, M.P., Hulshoff Pol, H.E., 2010. Exploring the brain network: a review on resting-state fMRI functional connectivity. Eur. Neuropsychopharmacol. 20, 519–534.
Van Veen, B.D., van Drongelen, W., Yuchtman, M., Suzuki, A., 1997. Localization of brain electrical activity via linearly constrained minimum variance spatial filtering. IEEE Trans. Biomed. Eng. 44, 867–880.
van Wijk, B.C., Stam, C.J., Daffertshofer, A., 2010. Comparing brain networks of different size and connectivity density using graph theory. PLoS One 5, e13701.
van Wijk, B.C., Beek, P.J., Daffertshofer, A., 2012. Neural synchrony within the motor system: what have we learned so far? Front. Hum. Neurosci. 6, 252.
Varela, F., Lachaux, J.P., Rodriguez, E., Martinerie, J., 2001. The brainweb: phase synchronization and large-scale integration. Nat. Rev. Neurosci. 2, 229–239.
Vartiainen, J., Liljestrom, M., Koskinen, M., Renvall, H., Salmelin, R., 2011. Functional magnetic resonance imaging blood oxygenation level-dependent signal and magnetoencephalography evoked responses yield different neural functionality in reading. J. Neurosci. 31, 1048–1058.
Whittington, M.A., Traub, R.D., Kopell, N., Ermentrout, B., Buhl, E.H., 2000. Inhibition-based rhythms: experimental and mathematical observations on network dynamics. Int. J. Psychophysiol. 38, 315–336.
Winterer, G., Carver, F.W., Musso, F., Mattay, V., Weinberger, D.R., Coppola, R., 2007. Complex relationship between BOLD signal and synchronization/desynchronization of human brain MEG oscillations. Hum. Brain Mapp. 28, 805–816.
Wu, C.W., Gu, H., Lu, H., Stein, E.A., Chen, J.H., Yang, Y., 2008. Frequency specificity of functional connectivity in brain networks. NeuroImage 42, 1047–1055.
Xiang, H.D., Fonteijn, H.M., Norris, D.G., Hagoort, P., 2010. Topographical functional connectivity pattern in the perisylvian language networks. Cereb. Cortex 20, 549–560.
Xu, P., Huang, R., Wang, J., Van Dam, N.T., Xie, T., Dong, Z., Chen, C., Gu, R., Zang, Y.F., He, Y., Fan, J., Luo, Y.J., 2014. Different topological organization of human brain functional networks with eyes open versus eyes closed. NeuroImage 90, 246–255.
Zalesky, A., Fornito, A., Harding, I.H., Cocchi, L., Yucel, M., Pantelis, C., Bullmore, E.T., 2010. Whole-brain anatomical networks: does the choice of nodes matter? NeuroImage 50, 970–983.
Zalesky, A., Cocchi, L., Fornito, A., Murray, M.M., Bullmore, E., 2012. Connectivity differences in brain networks. NeuroImage 60, 1055–1062.